RSC Advances

PAPER

View Article Online
View Journal | View Issue

Cite this: *RSC Adv.*, 2025, **15**, 14170

Phytochemical-assisted synthesis, optimization, and characterization of silver nanoparticles for antimicrobial activity†

Cynthia A. Gwada,[ab] Prince S. Ndivhuwo,[cd] Kabo Matshetshe,[d] Emily Aradi,[e] Phumlane Mdluli,[c] Nosipho Moloto,[b] Francis Otieno[a] and Mildred Airo *[a]

The increasing prevalence of antimicrobial resistance (AMR) bacteria poses a major global health threat, compounded by the limited development of new antibiotics. To address this challenge, alternative strategies, including nanoparticle-based therapies, are being explored. This study investigates the antimicrobial properties of green-synthesized silver nanoparticles (AgNPs) derived from leaf extracts of *Ocimum gratissimum* (OG), *Apium graveolens* (AG), and *Aloe arborescens* (AA). These plant extracts act as reducing, capping, and stabilizing agents during the synthesis process. By controlling the reaction parameters, the synthesized AgNPs displayed surface plasmon resonance (SPR) peaks at 434, 427, and 435 nm for OG, AG, and AA, respectively, indicating successful nanoparticle formation. The particles were predominantly spherical, with average sizes of 28.5 ± 6.3 nm (AgNPs-OG), 15.07 ± 3.8 nm (AgNPs-AA), and 20.2 ± 2.5 nm (AgNPs-AG), although some particles exhibited triangular and cylindrical shapes. X-ray diffraction (XRD) confirmed the formation of crystalline, face-centered cubic (FCC) metallic silver, while Fourier Transformation Infrared (FTIR) identified functional groups such as alcohols, amines, amides, carboxyl, and esters capping the surface of AgNPs. Energy dispersive spectroscopy (EDS) further confirmed the purity of the AgNPs. The antimicrobial activity of the synthesized AgNPs was tested against Gram-negative *E. coli* and Gram-positive *S. aureus* bacteria. Notably, AgNPs demonstrated high antimicrobial efficacy, particularly with smaller-sized, spherical particles showing superior performance. The minimum inhibitory concentration was as low as 1.016 μg mL^{-1}, highlighting the strong antimicrobial potential of AgNPs, whereas the minimum bactericidal concentration was recorded for *E. coli*, indicating greater susceptibility of Gram-negative bacteria to AgNPs and a concentration-dependent bactericidal effect. A comparison analysis showed that the antimicrobial effectiveness of the aqueous extract was significantly enhanced when AgNPs were incorporated, whereas higher antimicrobial performance was observed for green-synthesized AgNPs compared with wet chemically synthesized AgNPs reported in the literature. This is attributed to enhanced biocompatibility and a synergistic effect between the nanoparticles and plant-derived bioactive compounds. The mechanism of action of AgNPs involves silver ion (Ag^+) release and reactive oxygen species (ROS) generation *via* surface oxidation and photoactivation. These findings underscore the potential of green-synthesized AgNPs as an alternative strategy in mitigating AMR.

Received 19th December 2024
Accepted 10th April 2025

DOI: 10.1039/d4ra08900f

rsc.li/rsc-advances

1 Introduction

Antimicrobial resistance (AMR), also known as a 'silent pandemic', has become a growing threat to the effective treatment of infections caused by microorganisms. AMR leads to decreased efficacy of drugs targeting these infections, making patient treatment more challenging, expensive, or in some cases, impossible. With over 5 million deaths already attributed to AMR,[1] projections indicate that more than 40 million additional deaths could occur between now and 2050.[2] The increasing prevalence of antibiotic-resistant microorganisms has prompted a growing interest in alternative antimicrobial agents, such as AgNPs, which have shown remarkable antibacterial, antifungal,

[a]*School of Physical and Biological Sciences, Maseno University, Private Bag, Maseno, Kenya. E-mail: mildredairo@gmail.com; Tel: +25 4714979279; +27 73 761 0875*
[b]*Molecular Sciences Institute, School of Chemistry, University of the Witwatersrand, Private Bag 3, Wits, 2050, South Africa*
[c]*Health Platform, Advanced Materials Division, Mintek, 200 Malibongwe Drive, South Africa*
[d]*DSI/Mintek Nanotechnology Innovation Centre, Mintek, 200 Malibongwe Dr, Praegville, Randburg 2194, South Africa*
[e]*Henry Royce Institute, University of Manchester, Oxford Road, Manchester, M13 9PL, UK*

† Electronic supplementary information (ESI) available. See DOI: https://doi.org/10.1039/d4ra08900f

and antiviral properties.[3,4] AgNPs are known for their broad-spectrum antimicrobial activity, biocompatibility, and ease of synthesis, making them a promising candidate for a variety of medical, industrial, and environmental applications.[5]

The synthesis of AgNPs using green chemistry methods involving plant extracts has gained attention as an environmentally friendly and cost-effective alternative to traditional chemical processes.[6,7] In particular, the use of plant extracts for the biosynthesis of AgNPs has garnered attention due to the variety of bioactive compounds, including essential oils, flavonoids, and polysaccharides, that can serve as reducing and stabilizing agents in nanoparticle (NPs) formation[8–11] These compounds facilitate the reduction of silver ions (Ag^{+}) to silver atoms (Ag^{0}/AgNPs), subsequently enhancing their stability and improving their activity because of the functional groups attached to their surfaces.[11] Among the numerous plants with potential for NPs synthesis, *Ocimum gratissimum* (African basil), *Apium graveolens* (celery), and *Aloe arborescens* (a species of aloe) stand out for their rich chemical compositions and known antimicrobial properties.[12–14] Each of these plants contains a variety of bioactive compounds that exhibit antimicrobial, antioxidant, and anti-inflammatory activities. *Ocimum gratissimum* (abbreviated as, OG), for instance, is rich in essential oils like eugenol and methyl eugenol, which have demonstrated effective antimicrobial activity.[15] *Apium graveolens* (AG) contains volatile oils such as limonene and apiole, which also possess antimicrobial properties.[16] *Aloe arborescens* (AA), on the other hand, is known for its high content of polysaccharides like acemannan and anthraquinones, which have been shown to have significant antimicrobial and skin-healing effects.[17]

Although several studies have explored the potential of individual plants for synthesizing AgNPs,[18–20] direct comparisons of their effectiveness in NP formation and antimicrobial activities remain limited. The existing literature provides a solid foundation for understanding the comparative capabilities of different plant extracts in AgNP synthesis, highlighting key characteristics such as size, morphology, stability and antimicrobial properties.[21,22] However, there is a lack of comparative studies specifically evaluating OG, AG, and AA in this context. To address this gap, this study systematically investigates the ability of these three plant extracts to facilitate NPs synthesis and assesses their potential antimicrobial applications.

By synthesizing AgNPs using these plant extracts and assessing their antimicrobial activity, this project aims to enhance the understanding of how the chemical composition of each plant affects the properties and effectiveness of NPs against microbial pathogens. Specifically, the extracts from the leaf materials (as depicted in Fig. 1) of OG, AG, and AA were used to synthesize AgNPs. As part of an additional green chemistry strategy, water, a clean, safe, less expensive, and non-toxic solvent, was used to extract the active ingredients that were fundamental during NPs synthesis. The antimicrobial activity of the as-synthesized plant extract NPs was then tested against Gram-negative and Gram-positive bacteria. In addition to achieving green-synthesized NPs, the study aimed to enhance the antimicrobial performance of plant extracts using the NPs, thereby lowering the high concentrations typically reported in the literature[12–14] and improving the antimicrobial efficacy at low concentrations. Similarly, incorporating NPs into plant extracts was also intended to potentially reduce biotoxicity[23–25] and increase the biocompatibility of AgNPs.

2 Materials and methods

2.1 Materials

Silver nitrate ($AgNO_3 \geq 99.9\%$), Luria Bertani Broth (LB), Tryptic Soy Agar (TSA), and Petri dishes were purchased from Sigma-Aldrich, Germany, and used as received. Distilled (DI) water was used as a solvent. OG and AA plant materials were collected from the Maseno University farm, whereas AG was purchased from a local market around Maseno University. Gram-negative (*Escherichia. coli*) and Gram-positive (*Staphylococcus. Aureus*) bacteria strains were obtained from the DSI/Mintek Nanotechnology Innovation Centre and the Centre for Metal-based Drug Discovery, South Africa.

2.2 Plant extract preparation

The collected fresh leaves of OG, AG, and AA were washed several times with DI water to remove the surface dirt and inorganic impurities. The leaves were then dried at room temperature for approximately 72 h. The dried leaves were crushed into fine powder using a Sayonapps blender. The prepared samples were then packed in air-tight bags for extraction purposes. 2.5 g of crushed leaves were boiled

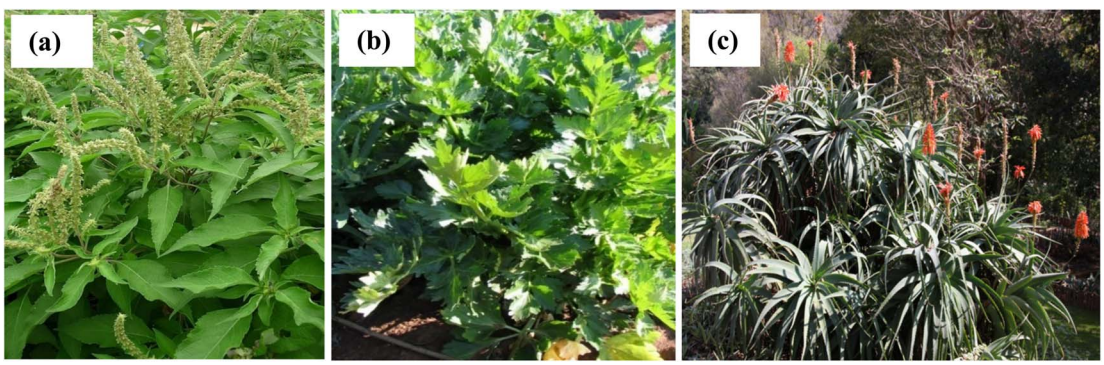

Fig. 1 Photographic representations of (a) OG, (b) AG, and (c) AA, plant materials.

separately in 100 mL of DI water for approximately 20 min. The resultant extract was subsequently filtered through Whatman No. 1 filter paper using a Buchner funnel, followed by centrifugation at 5000 rpm for 10 min. Clear supernatants were collected and stored at 4 °C until further use in the synthesis of AgNPs.

2.3 Synthesis of AgNPs using AA, OG, and AG leaf extracts

A one-pot colloidal synthesis method was used to fabricate AgNPs. In this process, approximately 70 mL of DI water was heated to 80 °C in a round-bottom three-neck flask with continuous stirring under reflux. Next, 0.102 g (6 mM) of $AgNO_3$ dissolved in 10 mL of DI water and 20 mL of OG-leaf extract were added to the flask in a 20 : 80 volume ratio (plant extract to silver ions). A reduction in the reaction temperature and color change from colorless to pale yellow were then observed. The solution was then stabilized at 75 °C, and aliquots were collected at 15, 30, and 60 minutes of synthesis. Each aliquot was allowed to cool to room temperature before the characterization of AgNPs-OG and further applications. The procedure was repeated at room temperature (25 °C) and 50 °C. Additionally, at 75 °C, reactions were conducted with $AgNO_3$ concentrations of 1 mM and 3 mM, and plant extract to silver nitrate solution ratios of 5 : 95 and 10 : 90. Following the same procedure, AgNPs-AA and AgNPs-AG were synthesized at 75 °C for 60 minutes, with a 6 mM concentration of $AgNO_3$ and a plant extract to $AgNO_3$ solution ratio of 20 : 80.

2.4 Use of the well-diffusion method

The as-synthesized AgNPs were evaluated using the well-diffusion method for their antibacterial efficacy against Gram-positive *S. aureus* and Gram-negative *E. coli*. To ensure homogeneous distribution, 20 mL of TSA medium was added to sterilized plates. Using an L-shaped cell spreader, about 100 μL (1×10^6 CFU mL^{-1}) of each bacterial strain was evenly distributed onto TSA plates. Using a cork borer, wells were created on the plates, followed by loading 100 μL of AgNPs (65 μg mL^{-1}) solution. The wells were incubated for 24 h at 37 °C. A ruler was used to obtain the disc scale, and ImageJ and Origin software were used to calculate the length of the inhibition zones. The experiment was performed in triplicate.

2.5 Assay of minimum inhibitory concentration (MIC)

The MIC of the synthesized AgNPs was determined using a standard broth dilution method.[4] About 2 mL (65 μg mL^{-1}) of either AgNPs-AA, AgNPs-OG, or AgNPs-AG was loaded into a 2 mL LB broth solution dispensed inside sterilized test tubes. Two-fold dilution methods were used to obtain concentrations of 0.254, 0.508, 1.016, 2.031, 4.063, 8.125, 16.25, and 32.5 μg mL^{-1}. The McFarland method was used to adjust the bacterial concentration to 1×10^6 CFU mL^{-1}. A 10 μL inoculum of either *S. aureus* or *E. coli* was added to each tube. The tubes were gently mixed and then incubated for 24 h at 37 °C with shaking at 250 rpm. The MIC is the lowest concentration of the plant-based AgNPs that inhibits the visible growth of bacteria.

2.6 Minimum bactericidal concentration (MBC)

After the MIC determination of AgNPs, aliquots of 10 μL of the materials from the tubes that showed no visible bacterial growth were cultured on TS agar plates and incubated for 24 h at 37 °C, after which observations were made for the presence or absence of bacterial growth. MBC is the lowest concentration of an antimicrobial agent that kills 99.9% of the initial bacterial population.

2.7 Characterization of as-synthesized silver nanoparticles

The Ocean View Optics FLMT11918 UV-VIS-NIR spectrophotometer was used to perform optical measurements of the as-synthesized AgNPs. The measurements were performed on samples placed in quartz cuvettes (1 cm, path length) using distilled water as a reference solvent. The size and shape of AgNPs were determined using FEI Talos F200A AEM +X-FEG+ Super-x at the University of Manchester. A portion of the sample (AgNPs-OG, AgNPs-AG, and AgNPs-AA) was sonicated and deposited onto a TEM grid, which was then left to air-dry before analysis. The operation was performed in TEM mode with a beam spot size of 20–100 nm and an electron acceleration voltage of 200 kV. The elemental analysis of the NPs was performed using Scanning Transmission Electron-Energy-Dispersive Spectroscopy (STEM-EDS). The STEM-EDX spectrum image data were acquired using a dwell time of 200 μs per pixel (over a 512 by 512 pixels area) with a total acquisition time per dataset of ~35 to 40 minutes, and data were processed using Velox 2.6 software. The shapes were determined visually, and the particle sizes were measured using ImageJ software. Grains of more than 100 (of different samples) were measured from the TEM images, and the average size was reported. The analysis of bioactive functional groups on the surface of plant-based AgNPs was conducted using a Bruker Tensor 27 Fourier Transform Infrared (FTIR) spectrometer. The samples were first centrifuged, and the concentrated residue was collected and dispersed in ethanol. After air-drying, their spectral wavelengths were obtained between 4000 and 400 cm^{-1} range. The crystallinity and phase structure of the dried samples were investigated using a Bruker D2 Phaser XRD with Cu Kα radiation source ($\lambda = 1.54056$) at 30 kV and 10 mA.

3 Results and discussions

3.1 Effect of reaction parameters on optical properties of AgNPs

The effects of various parameters on the properties of AgNPs were initially explored using OG extract to identify the conditions for NP synthesis. The absorption spectra of the monitored parameters are presented in Fig. 2. Reaction temperatures were adjusted to 25 °C, 50 °C, and 75 °C, with corresponding SPR peaks observed at 431 nm, 429 nm, and 426 nm, respectively. A blue shift in the SPR peak with increasing temperature indicates the formation of smaller NPs.[26] At a lower temperature (25 °C), the reduced kinetic energy results in a slower nucleation rate because fewer atoms acquire enough energy to overcome the activation barrier. This leads to fewer nuclei and slower

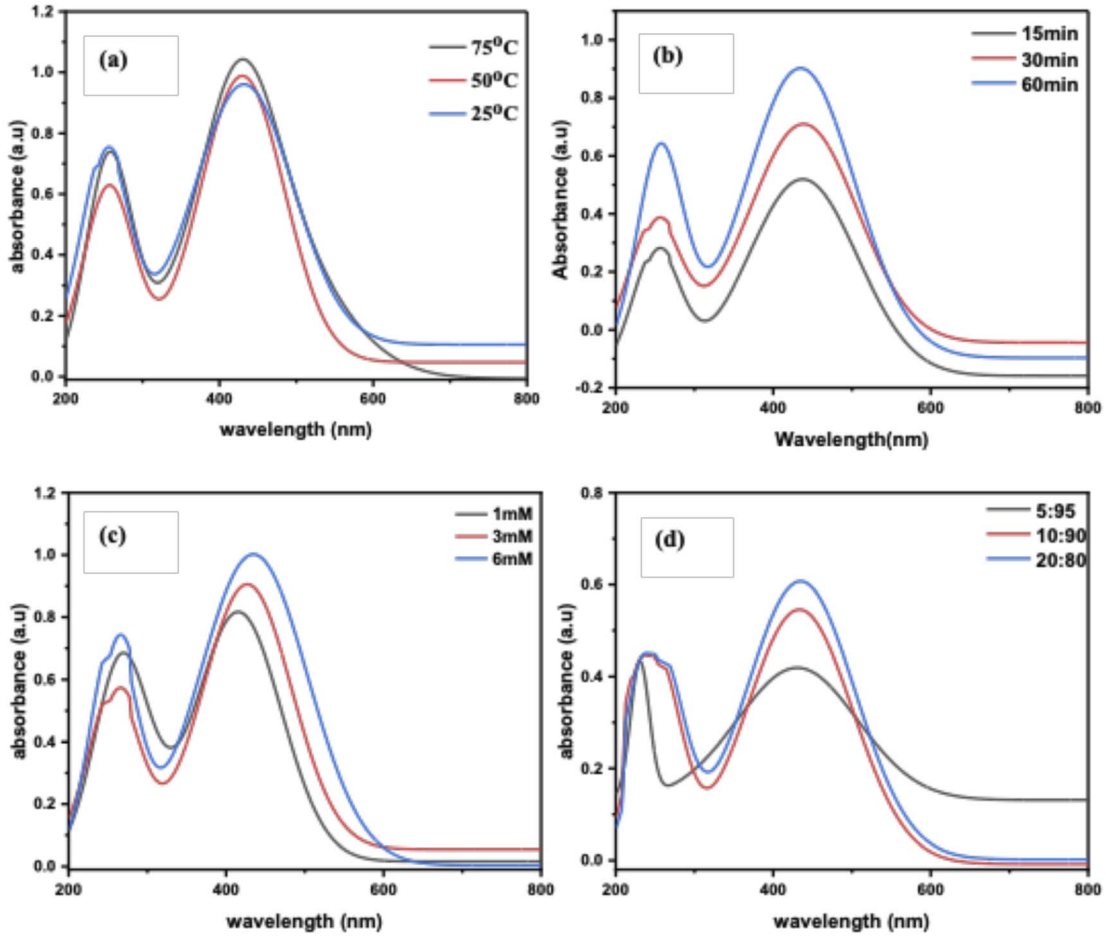

Fig. 2 UV-vis spectra of AgNPs synthesized using OG plant extract under varying conditions: (a) reaction temperature (b) time, (c) $AgNO_3$ concentration, and (d) plant extract to silver ion volume ratio.

diffusion and the growth of larger, more polydisperse NPs. As the temperature rises, the increased kinetic energy accelerates nucleation, resulting in the formation of many small nuclei that rapidly grow into smaller NPs.[27] Additionally, SPR peaks were recorded at 437, 438, and 440 nm for reaction times of 15, 30, and 60 min, respectively, at 75 °C. The observed redshift suggests an increase in NPs size due to the Ostwald ripening process,[28] where larger particles grow at the expense of smaller ones. When the $AgNO_3$ concentration was varied, SPR peaks were observed at 415, 426, and 434 nm for 1 mM, 3 mM, and 6 mM, respectively, at 75 °C for 60 min. The redshift with increasing $AgNO_3$ concentration indicates the formation of relatively larger NPs because higher monomer concentrations lead to a rapid burst of nucleation, producing more nuclei that grow into larger NPs.[29] Finally, SPR peaks were recorded at 430, 433, and 434 nm for volume ratios of plant extract to silver ions of 5 : 95, 10 : 90, and 20 : 80, respectively, at 75 °C for 60 min with a concentration of 6 mM $AgNO_3$, indicating a higher concentration of NPs. This suggests that a greater abundance of active phytochemicals in the extract enhances the reduction and capping ability of NPs.[30]

Notably, the intensity of the SPR peak of AgNPs is primarily related to the size and concentration of the particles, with larger and more concentrated NPs generally producing stronger SPR signals. The peak position (wavelength) and intensity are also affected by the shape of the NPs and the properties of the surrounding environment.[31] For the sake of this study, the conditions that produced NPs with the highest intensity were used as a template for synthesis using the other two plant extracts AA and AG. Therefore, AgNPs-AA and AgNPs-AG were synthesized at 75 °C temperature for 60 min using 6 mM $AgNO_3$ concentration, and a 20 : 80 mL plant extract to silver ion volume ratio.

3.2 Visual characterization

The plant leaf extract was used as a reducing, capping, and stabilizing agent. The antioxidant properties of the bioactive compounds present in these extracts chemically transform $AgNO_3$ into active species (monomers), which then form nanocrystals that grow in the presence of organic surfactants from the plant extract. The addition of plant extract to $AgNO_3$ induces a distinct colour change from pale yellow to dark brown, as illustrated in Fig. 2a–c. The color change indicates the reduction of monovalent silver ion (Ag^+) from silver salt solution to zero-valent silver (Ag^0), forming AgNPs. This phenomenon occurs due to SPR, in which free-moving, unbound electrons on

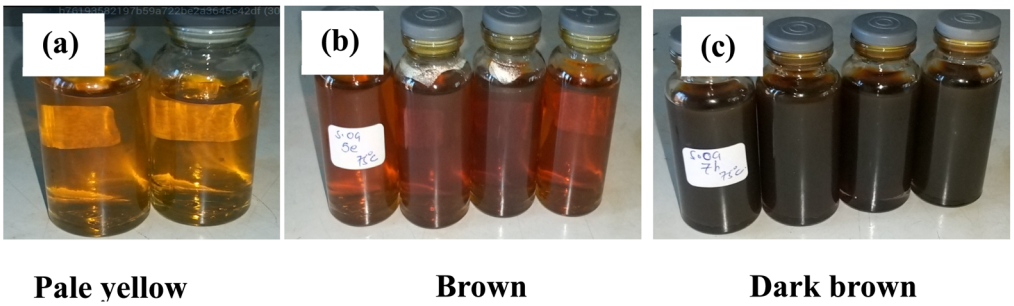

Fig. 3 Photographic representation of sequential color changes observed during the synthesis of AgNPs using OG extract at a temperature of 75 °C and time (a) 15 min, (b) 30 min and (c) 60 min.

the surface of NPs collectively oscillate in response to light.[32] Similar findings were reported by Chakravarty, Ahmad,[33] Pratim Sarma, Barman,[34] and Saygi, Bayram,[35] who synthesized AgNPs using fruit extracts of *Syzygium cumini*, leaf extract of *Murraya koenigii* and flower petals of *Cynara scolymus* L., respectively. The observed color change confirmed the successful synthesis of AgNPs.[36] The same trend in color change was observed in AgNPs synthesized using AG and AA when the reaction duration was changed over one hour period. The synthesized NPs were subsequently subjected to further characterization, as detailed below (Fig. 3).

3.3 Structural properties of AgNPs

FTIR was employed to investigate the functional groups capping the surface of the synthesized AgNPs, as depicted in Fig. 4. The notable absorption bands observed were as follows: a band at around 3290 cm^{-1} corresponds to the O–H stretch of carboxylic acids. The band at 2890 cm^{-1} is attributed to the C–H stretching of aromatic compounds and alkenes. The notable band at approximately 2340 cm^{-1} represents the –N=C=O stretch of isocyanates and the –C≡N stretch of nitriles. The band observed at around 2101 cm^{-1} indicates the C≡C stretch of alkynes. The band at around 1860 cm^{-1} corresponds to the C=O stretching of acid anhydrides. The band at 1663 cm^{-1} is attributed to the C=O stretch of amides (amide I, secondary or tertiary), which is coupled with a band at 1528 cm^{-1}, corresponding to the N–H stretch of amides and possibly the NO_2 stretch of nitro groups. The band at 1370 cm^{-1} corresponds to the O–H bending (in-plane) of alcohols and phenols. The band at 1184 cm^{-1} indicates an O–C stretch of the esters. The notable band at approximately 1019 cm^{-1} represents the C–N stretching vibrations of primary or secondary amines. Bands below 1000 cm^{-1} correspond to out-of-plane C–H bending vibrations. These absorption bands suggest the presence of functional groups such as phenols, alcohols, esters, amides, amines, carboxylic acids, acid anhydrides, alkyl groups, and aromatic compounds attached to the surface of AgNPs.

PXRD was used to investigate the crystallinity and phase structure of the synthesized AgNPs, as shown in Fig. 5. The diffraction peaks observed at 2θ values of 38.10°, 44.60°, 64.67°, 77.55°, and 81.50° were indexed to the (111), (200), (220), (311), and (222) planes, respectively, corresponding to the face-centered cubic (FCC) crystal structure of the pure silver metal according to the JCPDS file (No. 00-001-1167). The space group associated with this structure is $Fm\bar{3}m$ (225). The high peak

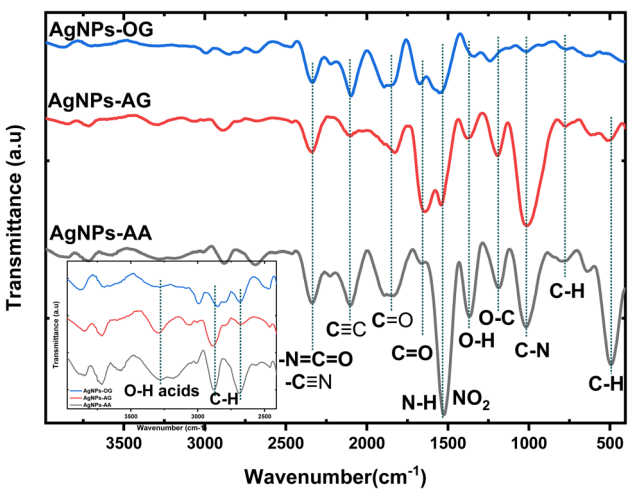

Fig. 4 FTIR spectra showing the functional groups capping the surfaces of the three synthesized AgNPs.

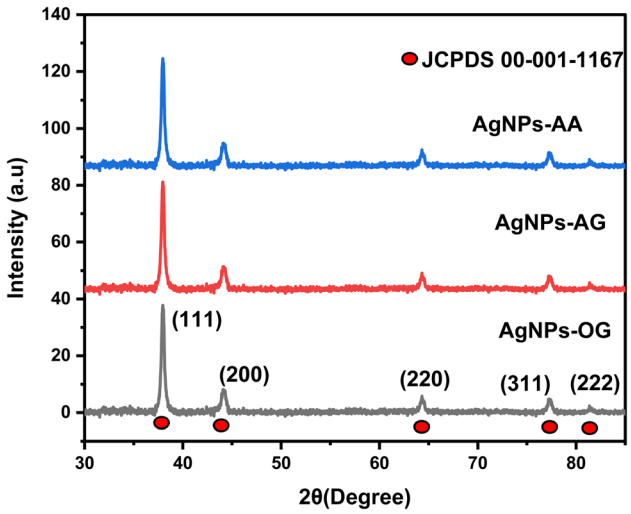

Fig. 5 XRD crystallographic patterns showing the phase structures of the synthesized AgNPs.

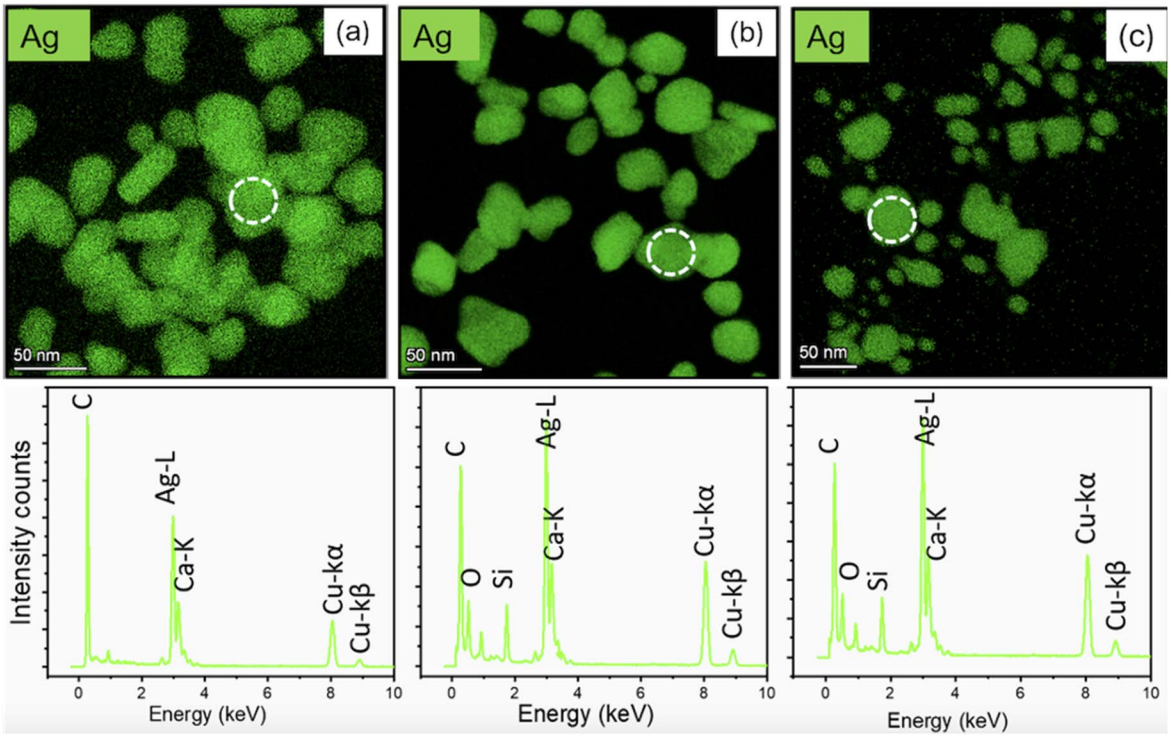

Fig. 6 STEM-EDS elemental mapping of (a) AgNPs-OG, (b) AgNPs-AA, (c) AgNPs-AG, and the corresponding EDS spectra showing the elemental composition of the synthesized samples.

intensity indicates a high degree of crystallinity in the formed NPs.

The composition of the as-synthesized AgNPs was confirmed using STEM-EDS, as shown in Fig. 6. The elements observed in the material include silver, carbon, oxygen, copper, and traces of silicon and calcium, where the Cu signal originates from the copper grid used during sample preparation. The presence of oxygen and carbon likely results from the oxygen- and carbon-containing functional groups in the plant extract used for synthesis. Traces of silicon and calcium may be attributed to impurities introduced during sample preparation for STEM-EDS analysis. A prominent peak at 3 KeV corresponding to the Lα line qualitatively confirms the presence of metallic silver in the AgNPs. Overall, the analysis indicated that approximately 99% of the material consisted of silver, which aligns with the observed SPR peak in the UV-vis spectrum.

3.4 Morphological properties

The TEM micrographs shown in Fig. 7 illustrate the size and shape distribution of AgNPs obtained using the three plant extracts. The dominant spherical-like shape was observed. The recorded average particle sizes were 28.5± 6.3 nm (AgNPs-OG), 15.07 ± 4.8 nm (AgNPs-AA), and 20.2 ± 2.5 nm (AgNPs-AG). The NPs were noted to be polydisperse, as indicated by the high standard deviations observed in the size measurements. The irregularity in shapes is attributed to the selective coordination of various functional groups, such as carbonyl (C═O), carboxyl (–COOH), amine ($–NH_2$), and hydroxyl (–OH) from the plant extract, with the surface atoms of the forming NPs. This selective coordination can either hinder or promote growth in specific directions, leading to anisotropic shapes such as triangles, rods, and cylindrical forms.[37]

3.5 Optical properties

Absorption spectroscopy was used in this study to examine the optical properties of the synthesized AgNPs, and the plant extract and their respective spectra are shown in Fig. 8. A characteristic SPR peak was observed at 434, 427, and 435 nm for AgNPs-OG, AgNPs-AG, and AgNPs-AA, respectively. The SPR peak occurs when the AgNPs are exposed to incident light, causing the free electrons on the surface of the AgNPs to collectively oscillate. This oscillation produces electric fields around the metal–dielectric interface when the incoming photon energy matches the frequency of the oscillating electrons.[32] There was no significant difference in the SPR peak position despite the difference in the sizes of the NPs, a phenomenon that may be attributed to the presence of organic molecules from plant extracts, as they adsorb on the surface of the NPs. These molecules can influence the surface plasmon resonance by altering the dielectric environment, potentially masking the effect of particle size on the SPR peak.[38,39] In this case, the interaction between AgNPs and organic molecules may alter the overall SPR behavior in ways that make size differences less pronounced. Additionally, broadening of the SPR peak was observed, as the full width at half maximum (FWHM) values for AgNPs-OG, AgNPs-AG, and AgNPs-AA were 186, 318, and 338 nm, respectively. These values indicate the polydispersity of the NPs, which is consistent with

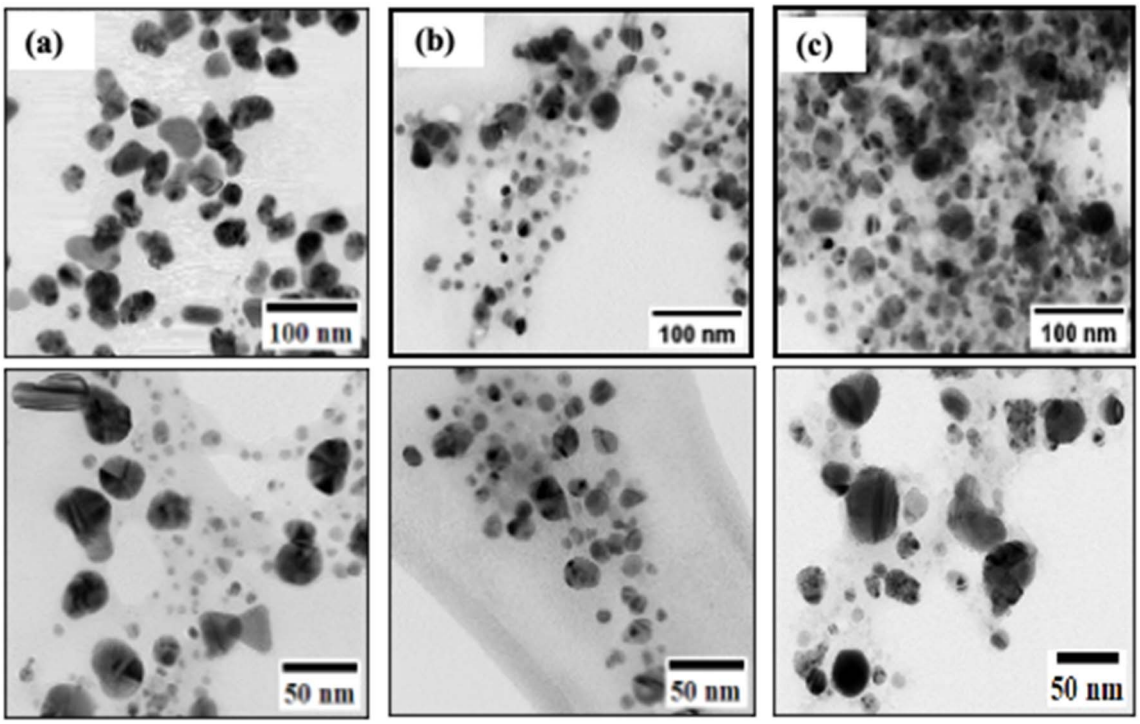

Fig. 7 TEM micrographs of (a) AgNPs-OG, (b) AgNPs-AA, and (c) AgNPs-AG, illustrating the particle size, shape, and distribution at high (top) and low (bottom) magnifications, respectively.

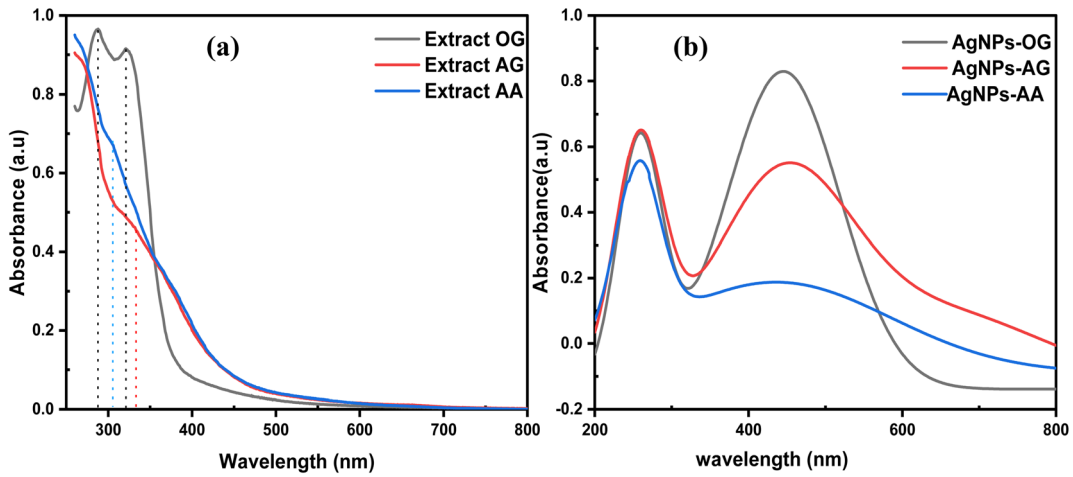

Fig. 8 Absorption spectra of (a) plant extract and (b) AgNPs synthesized from the extracts of the three plants.

the findings from the TEM analysis. From the values of the FWHM, it can be deduced that the OG extract produced more significantly uniform NPs followed by AG extract than AA extract, a phenomenon that may be attributed to the different bioactive groups found in the different plants as presented by the FTIR spectra thereby presenting differences in binding and reducing Ag^{+} capabilities. From the literature, the broadening of the SPR peak is an indication of possible different size and shape distributions, aggregation and the existence of surface defects in the NPs.[40,41] The TEM micrographs and FWHM values indicate that the SPR peak broadening may be associated with the size and shape distribution. Further, the size of the NPs is a known factor that affects the intensity of the SPR peak. Smaller NPs typically have weaker SPR peak intensities due to fewer surface atoms, less efficient plasmon coupling, and higher curvature and surface-to-volume ratios. In contrast, larger NPs generally exhibit stronger and sharper SPR peaks because they have more surface atoms for plasmon excitation, although very large NPs may experience redshift and peak broadening due to increased damping and reduced plasmonic coupling efficiency.[42,43] Thus, larger AgNPs-OG showed a slightly intense and narrow SPR peak, followed by AgNP-AG and then

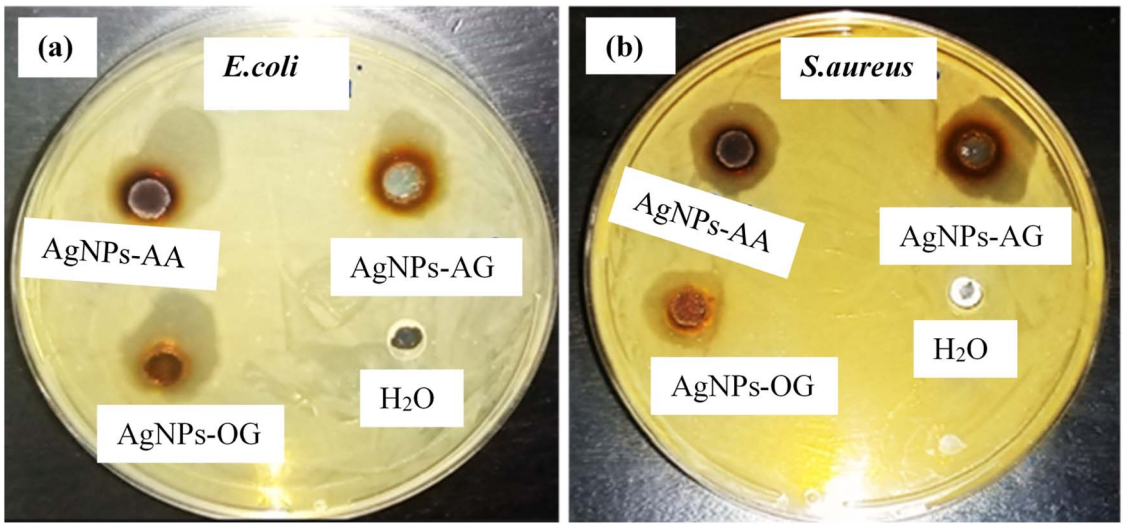

Fig. 9 Visible inhibitory Zones generated by AgNPs-AA, AgNPs-AG, and AgNPs-OG against (a) *E. coli* and (b) *S. aureus*.

AgNP-AA based on their sizes from TEM analysis. Finally, the shoulder bands in the 270–300 nm range of the spectra in Fig. 8b correspond to the π–π * absorption of various chromophores, such as –C═O, –NH_2, –C≡N, and –NO_2,[44] present in the bioactive molecules from the plant extracts that are involved in capping the AgNPs. Fig. 8a shows that the peaks between 270 and 300 range belonged to the plant extract.

3.6 Antimicrobial activity of AgNPs

The well-diffusion method was used to determine the antimicrobial activity of the synthesized AgNPs. As shown in Fig. 9, visible inhibition zones were generated, whereas Table 1 summarizes the measured inhibition zones (mean ± standard deviation(SD)). Water was used as a negative control. A higher inhibitory effect was observed for *E. coli* than for *S. aureus.* This difference is attributed to variations in cell structure. Gram-negative bacteria, such as *E. coli*, have a thin peptidoglycan layer and a thick layer of lipopolysaccharide (LPS) (endotoxin) in the outer cell membrane, which makes them susceptible to AgNPs. In contrast, Gram-positive bacteria, like *S. aureus,* have a thicker peptidoglycan layer and a thinner LPS layer. The thicker peptidoglycan layer in Gram-positive bacteria acts as a barrier, reducing the penetration ability of AgNPs into the cells.[4]

A two-fold dilution method was used to determine the MIC of AgNPs, with a summary outlined in Table 1. AgNPs demonstrated effectiveness at concentrations of 1.016 and 2.031 μg mL^{-1} when varying concentrations (0.254, 0.508, 1.016, 2.031,4.063, 8.125, 16.25, and 32.5 μg mL^{-1}) were tested. The high antimicrobial performance observed for AgNPs-AA and relatively AgNPs-AG compared to AgNPs-OG is attributed to the smaller NP sizes as well as the functional groups attached to the surfaces of the NPs. Smaller NPs can penetrate the cell membrane, causing the release of Ag^+. Ag^+ then binds to and interacts with vital cell biomolecules, such as proteins, amino acid residues, and DNA, causing toxicity. Additionally, the spherical sizes of AgNPs-AA and AgNPs-AG provide a larger surface area for the generation of Ag^+ ions, enhancing their antimicrobial activity compared to the anisotropic shapes observed in AgNPs-OG. The functional groups on the surfaces of the NPs also contribute to their superior performance against bacteria. Although plants appear to have similar functional groups as observed in FT-IR analysis, the high intensity of phytochemicals such as O–H, N–H, and C═O in Ag-AA can be attributed to their superior antimicrobial performance.[45]

To prevent the possibility of misinterpretation due to the turbidity of insoluble compounds in the broth dilution tubes, the MBC was determined. Approximately 10 μL of the samples from the tubes that showed no visible growth were cultured on TS agar plates and incubated at 37 °C for 24 hours. The observations summarized in Table 1 revealed no visible growth at higher concentrations of AgNPs in the case of Gram-negative *E. coli*, while visible growth was observed in all plates for Gram-positive *S. aureus*. This suggests that *E. coli* is more sensitive to AgNPs than *S. aureus.*

Table 1 Summary of the inhibition zone, MIC, and MBC of AgNPs

	Zone of inhibition (mm)		MIC (μg mL^{-1})		MBC (μg mL^{-1})	
Sample	*E.coli*	*S. aureus*	*E. coli*	*S. aureus*	*E. coli*	*S. aureus*
AgNPs-AA	17.5 ± 0.5	14.5 ± 0.6	1.016	1.016	32.5	—
AgNPs-OG	17.4 ± 0.3	12.8 ± 0.5	2.031	2.031	32.5	—
AgNPs-AG	16.1 ± 0.3	16.4 ± 0.1	1.016	2.031	32.5	—

3.7 Comparative studies

Table 2 presents a comparative analysis of the antimicrobial performance of the synthesized AgNPs *versus* the aqueous plant extract reported in the literature. The enhanced antimicrobial efficacy observed when AgNPs are incorporated into the aqueous plant extract is attributed to the synergistic effect

Table 2 Comparative test of inhibition zone, MIC, and MBC of the synthesized AgNPs with the plant extracts reported in the literature

	Zone of inhibition (mm)		MIC (μg mL^{-1})		MBC (μg mL^{-1})		
Sample	*E. coli*	*S. aureus*	*E. coli*	*S. aureus*	*E. coli*	*S. aureus*	References
AA extract	15.0 ± 2.0	4.0 ± 1.0	—	—	—	—	14
OG extract	14.0 ± 0.0	12.0 ± 0.2	50 000	100 000	—	—	12
AG extract	11.0 ± 1.2	13.4 ± 1.5	1250	1250	—	—	13
Incorporation of AgNPs							
AgNPs-AA	17.5 ± 0.5	14.5 ± 0.6	1.016	1.016	32.5	—	This study
AgNPs-OG	17.4 ± 0.3	12.8 ± 0.5	2.031	2.031	32.5	—	This study
AgNPs-AG	16.1 ± 0.3	16.4 ± 0.1	1.016	2.031	32.5	—	This study

Table 3 Comparative test of inhibition zone, MIC, and MBC of green-synthesized AgNPs with the chemical-based AgNPs reported in the literature

	Zone of inhibition (mm)		MIC (μg mL^{-1})		MBC (μg mL^{-1})		
Sample	*E. coli*	*S. aureus*	*E. coli*	*S. aureus*	*E. coli*	*S. aureus*	References
Phytochemical synthesis of AgNPs							
AgNPs-AA	17.5 ± 0.5	14.5 ± 0.6	1.016	1.016	32.5	—	This study
AgNPs-OG	17.4 ± 0.3	12.8 ± 0.5	2.031	2.031	32.5	—	This study
AgNPs-AG	16.1 ± 0.3	16.4 ± 0.1	1.016	2.031	32.5	—	This study
Wet chemical synthesis of AgNPs							
AgNPs-$NaBH_4$	1.4	1.1	—	—	—	—	46
AgNPs-ascorbic acid	—	—	156	312	—	—	47
TA-AgNPs	3.8	1.7	16	32	—	—	48

between the antimicrobial properties of AgNPs and the bioactive compounds present in the extract. Table 3 presents a comparative evaluation of the antimicrobial performance of the green-synthesized AgNPs obtained in this study and the chemically synthesized AgNPs reported in the literature. The superior antimicrobial performance of green-synthesized AgNPs is attributed to their increased biocompatibility with cell membranes and the synergistic effect of the antimicrobial properties of AgNPs and the phytochemicals from the plant extract. The observed high antimicrobial performance of the green-synthesized AgNPs at low concentrations potentially minimizes their biotoxicity to the cellular structure, making them potentially suitable for *in vivo* applications. A comparative study with the existing literature (Table 4) was also conducted to evaluate the performance of the AgNPs synthesized in this study relative to previous studies. Notably, the AgNPs produced using the green colloidal synthesis method exhibit comparable efficacy against the investigated pathogens. Furthermore, their performance was consistent across the different assays used to assess therapeutic effectiveness, a distinction not observed in previous studies.

Table 4 Comparison of the antibacterial efficacy of the synthesized AgNPs in this study with those reported in the literature

		Zone of inhibition (mm)		MIC (μg mL^{-1})		MBC		
Sample	Synthesis method	*E.coli*	*S.aureus*	*E.coli*	*S.aureus*	*E.coli*	*S.aureus*	References
Literature								
AgNPs-OG	Laminar air flow synthesis	20 ± 0.32	13 ± 0.2	—	—	—	—	22
AgNPs-AA	Sunlight synthesis	—	13 ± 0.5	—	—	—	—	21
AgNPs-AG	—	—	—	—	—	—	—	No studies to the best of our knowledge
Current study								
AgNPs-AA	Colloidal synthesis	17.5 ± 0.5	14.5 ± 0.6	1.016	1.016	32.5	—	This study
AgNPs-OG		17.4 ± 0.3	12.8 ± 0.5	2.031	2.031	32.5	—	This study
AgNPs-AG		16.1 ± 0.3	16.4 ± 0.1	1.016	2.031	32.5	—	This study

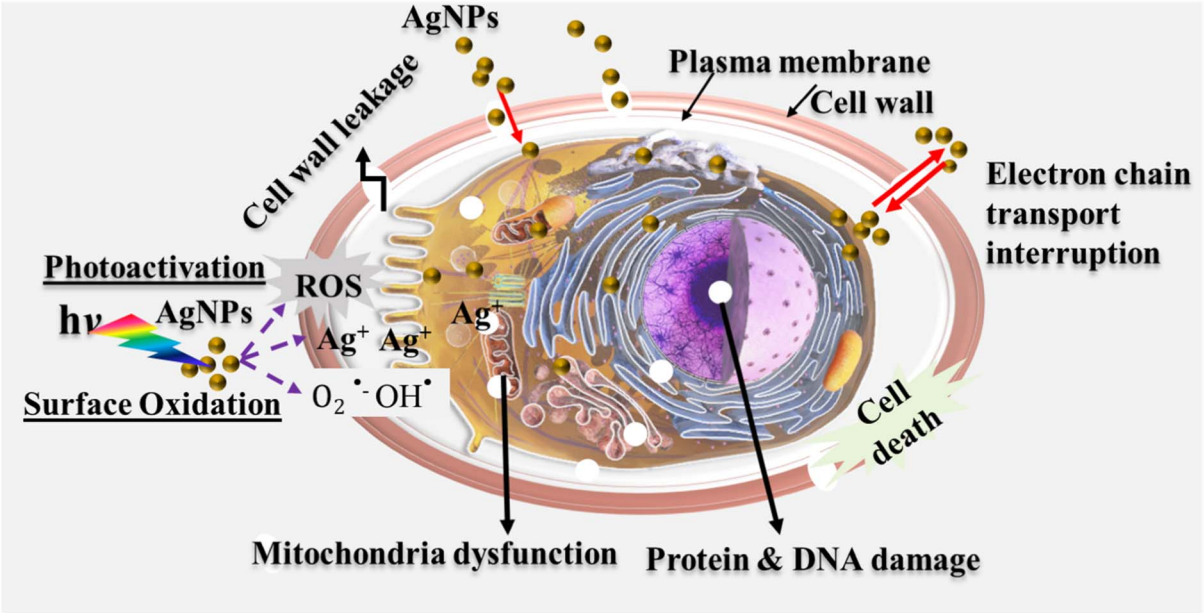

Fig. 10 Schematic illustration of the antibacterial mechanism of action of AgNPs.

3.8 Mechanism of action

The antimicrobial effectiveness of AgNPs can be primarily due to their high surface area-to-volume ratio and nanoscale properties, which allow them to interact with cell components, interfering with the cell machinery, and potentially causing toxicity (Fig. 10). The binding ability of nanoparticles through electrostatic interactions,[49] penetration, and adherence to bacterial cell walls causes morphological changes and damage to the cell wall and cytoplasmic components. The morphological changes experienced by the cell wall can increase the membrane permeability, causing irregular transport through the plasma membrane and leading to cell death. AgNPs can also undergo surface oxidation in the presence of water, body fluid, or tissue, generating bioactive Ag^+, which is more toxic to cells. The generated Ag^+ is more sensitive to the Sulphur (SH) containing groups such as proteins and DNA, causing disorder in regular functions, resulting in cellular toxicity and cell death. Moreover, the local surface plasmon resonance (LSPR) property of AgNPs contributes to the transfer of hot electrons to the cell metabolism of the microbes, releasing ROS such as H_2O_2, O_2^-, and $^{\bullet}OH$ with subsequent release of Ag^+.[50] The ROS can then bind covalently or non-covalently to cell macromolecules such as DNA and proteins, inducing toxicity by altering their normal functions.[51] Additionally, the high concentration of ROS in the bacterium results in an increase in oxidative stress, which damages the cytoskeleton, proteins, nucleic acid oxidation, and DNA replication, causing chromosomal aberrations and cell death.

4 Conclusions

This study successfully synthesized AgNPs using phytochemicals from *O. gratissimum*, *A. graveolens*, and *A. arborescens* extracts as reducing, capping, and stabilizing agents. Reaction conditions, including temperature, time, $AgNO_3$ concentration, and the volume ratio of plant extract to silver ions, were found to influence the properties of the AgNPs. Predominantly spherical NPs with triangular and cylindrical shapes were produced. The particles were noted to differ in size and were capped with functional groups such as alcohol, amine, amide, and carboxyl groups. Optical studies confirmed the successful synthesis of AgNPs through the observation of an SPR peak at distinct wavelengths. The characteristics of the SPR peak, including broadening and intensity, differed depending on the plant extract used for synthesis. Specifically, the SPR peak exhibited increasing broadening and intensity in the order: AgNPs-OG < AgNPs-AG < AgNPs-AA. The elemental analysis (EDS) showed that the material was primarily silver for all the plant extracts used. XRD analysis confirmed a highly crystalline FCC structure of silver. AgNPs displayed notable antimicrobial efficacy against *E. coli* and *S. aureus*, with superior activity observed in smaller, spherical NPs. The MIC was as low as 1.016 μg mL^{-1}, highlighting potent antimicrobial activity, and the MBC for *E. coli* demonstrated the heightened susceptibility of Gram-negative bacteria to AgNPs. All three plant-extract-synthesized AgNPs exhibited strong antimicrobial activity against the tested pathogens. However, their efficacy against *E. coli* followed the order: AgNPs-AA > AgNPs-AG ≫ AgNPs-OG, with a similar trend observed against *S. aureus*. This underscores the superior antibacterial potential of AgNPs-AA, making it a promising candidate for combating bacterial infections. The study also found that incorporating AgNPs into plant extracts significantly boosted the antimicrobial effect of the extracts, while functionalizing AgNPs with bioactive compounds enhanced the efficacy of chemically synthesized AgNPs at lower concentrations, potentially minimizing associated biotoxicity.

In conclusion, colloidal synthesis is an effective approach for synthesizing highly potent NPs with enhanced antibacterial properties. Following the necessary therapeutic assays for evaluating antimicrobial agents, this method is a promising strategy for developing efficient nanoparticle-based treatments against bacterial pathogens.

Data availability

All data underlying the results of this study are available in the figures and tables provided within this article.

Author contributions

Cynthia Gwada: conceptualization, methodology, investigation, data curation and writing of the original draft, preparation and editing. Nosipho Moloto and Emily Aradi: conceptualization, reviewing and editing. Mildred Airo and Francis Otieno: project administration, conceptualization, methodology, supervision, writing, reviewing and editing. Prince S. Ndivhuwo, Kabo Matshetshe and Phumlane Mdluli: Antibacterial experimental methodology, data curation, writing and editing.

Conflicts of interest

The authors declare no conflicts of interest.

Acknowledgements

The authors would like to acknowledge Maseno University and the University of Witwatersrand for providing laboratory space for bench work and access to characterization techniques. The DSI/Mintek Nanotechnology Innovation Center is acknowledged for providing the facilities for antimicrobial studies, and The University of Manchester for assistance with TEM characterization. This work was also funded by the TWAS-BMBF Seed Grant for New African Principal Investigators (SG-NAPI) grant number 4500474974 and the National Research Foundation (NRF) of South Africa.

References

1 C. Murray, *et al.*, Global burden of bacterial antimicrobial resistance in 2019: a systematic analysis, *Lancet*, 2022, **399**(10325), 629–655.
2 M. Naddaf, 40 million deaths by 2050: toll of drug-resistant infections to rise by 70%, *Nature*, 2024, **633**(8031), 747–748.
3 C. Liao, Y. Li and S. C. Tjong, Bactericidal and Cytotoxic Properties of Silver Nanoparticles, *Int. J. Mol. Sci.*, 2019, **20**(2), 449.
4 N. P. Shumbula, *et al.*, Investigation of Antimicrobial Activity and Cytotoxicity of Silver Nanoparticle Synthesized using Dopamine as a Reducing and Capping Agent, *ChemistrySelect*, 2024, **9**(12), e202303328.
5 V. Thamilselvi and K. Radha, A review on the diverse application of silver nanoparticle, *IOSR J. Pharm.*, 2017, **7**, 21–27.
6 S. Iravani, *et al.*, Synthesis of silver nanoparticles: chemical, physical and biological methods, *Res. Pharm. Sci.*, 2014, **9**(6), 385–406.
7 W. A. Shaikh, *et al.*, A review of the phytochemical mediated synthesis of AgNP (silver nanoparticle): the wonder particle of the past decade, *Appl. Nanosci.*, 2021, **11**(11), 2625–2660.
8 M. S. Al Aboody, Cytotoxic, antioxidant, and antimicrobial activities of Celery (Apium graveolens L.), *Bioinformation*, 2021, **17**(1), 147.
9 E. O. Igbinosa, *et al.*, In vitro assessment of antioxidant, phytochemical and nutritional properties of extracts from the leaves of Ocimum gratissimum (Linn), *Afr. J. Tradit. Complement. Altern. Med.*, 2013, **10**(5), 292–298.
10 S. Kumar and J. Yadav, Ethnobotanical and pharmacological properties of Aloe vera: a review, *J. Med. Plants Res.*, 2014, **48**(8), 1387–1398.
11 A. Zuhrotun, D. J. Oktaviani and A. N. Hasanah, Biosynthesis of Gold and Silver Nanoparticles Using Phytochemical Compounds, *Molecules*, 2023, **28**(7), 3240.
12 A. Ogodo, *et al.*, Activity of Leave and Stem Bark Cuttings of Ocimum gratissimum Extracts on Foodborne Pathogens, *J. Biol. Sci.*, 2017, **3**, 5–11.
13 A. Emad, *et al.*, Antioxidant, Antimicrobial Activities and Characterization of Polyphenol-Enriched Extract of Egyptian Celery (Apium graveolens L., Apiaceae) Aerial Parts via UPLC/ESI/TOF-MS, *Molecules*, 2022, **27**, 698.
14 F. Ghane, *et al.*, Antimicrobial Activity and Wound Healing Properties of Aloe Arborescens Extract: An in Vivo Study, *J. Adv. Biomed. Sci.*, 2023, **13**(2), 138–147.
15 C. V. Nakamura, *et al.*, Antibacterial activity of Ocimum gratissimum L. essential oil, *Mem Inst Oswaldo Cruz*, 1999, **94**(5), 675–678.
16 G. Nouioura, *et al.*, Exploring the essence of celery seeds (Apium graveolens L.): Innovations in microwave-assisted hydrodistillation for essential oil extraction using in vitro, in vivo and in silico studies, *Arabian J. Chem.*, 2024, **17**(5), 105726.
17 Y. Bai, *et al.*, A New Biomaterial Derived from Aloe vera-Acemannan from Basic Studies to Clinical Application, *Pharmaceutics*, 2023, **15**, 1913.
18 A. K. Giri, *et al.*, Green synthesis and characterization of silver nanoparticles using Eugenia roxburghii DC. extract and activity against biofilm-producing bacteria, *Sci. Rep.*, 2022, **12**(1), 8383.
19 M. Sharifi-Rad, H. S. Elshafie and P. Pohl, Green synthesis of silver nanoparticles (AgNPs) by Lallemantia royleana leaf Extract: Their Bio-Pharmaceutical and catalytic properties, *J. Photochem. Photobiol., A*, 2024, **448**, 115318.
20 M. A. Taleb Safa and H. Koohestani, Green synthesis of silver nanoparticles with green tea extract from silver recycling of radiographic films, *Results Eng.*, 2024, **21**, 101808.
21 S. S. D. Kumar, *et al.*, Cellular imaging and bactericidal mechanism of green-synthesized silver nanoparticles against human pathogenic bacteria, *J. Photochem. Photobiol., B*, 2018, **178**, 259–269.
22 K. Sharma, S. Guleria and V. Razdan, Green synthesis of silver nanoparticles using Ocimum gratissimum leaf

extract: characterization, antimicrobial activity and toxicity analysis, *J. Plant Biochem. Biotechnol.*, 2020, **29**, 213–224.
23 A. Barbasz, M. Oćwieja and M. Roman, Toxicity of silver nanoparticles towards tumoral human cell lines U-937 and HL-60, *Colloids Surf., B*, 2017, **156**, 397–404.
24 V. Bastos, *et al.*, The influence of Citrate or PEG coating on silver nanoparticle toxicity to a human keratinocyte cell line, *Toxicol. Lett.*, 2016, **249**, 29–41.
25 V. Bastos, *et al.*, Coating independent cytotoxicity of citrate- and PEG-coated silver nanoparticles on a human hepatoma cell line, *J. Environ. Sci.*, 2017, **51**, 191–201.
26 H. Liu, *et al.*, Effect of temperature on the size of biosynthesized silver nanoparticle: Deep insight into microscopic kinetics analysis, *Arabian J. Chem.*, 2020, **13**(1), 1011–1019.
27 V. Harish, Nanoparticle and Nanostructure Synthesis and Controlled Growth Methods, *Nanomaterials*, 2022, **12**(18), 3226.
28 A. M. Awuor, Synthesis and characterisation of metal selenide nanocrystals for use in electronic devices, PhD thesis, 2017.
29 M. Tesfaye, *et al.*, Green synthesis of silver nanoparticles using Vernonia amygdalina plant extract and its antimicrobial activities, *Heliyon*, 2023, **9**(6), e17356.
30 M. Rousta and N. Ghasemi, Green synthesis of silver nanoparticles using a mountain plant extract, *Rev. Roum. Chim.*, 2019, **64**, 143–152.
31 D. Paramelle, *et al.*, A rapid method to estimate the concentration of citrate capped silver nanoparticles from UV-visible light spectra, *Analyst*, 2014, **139**(19), 4855–4861.
32 F. Y. Alzoubi, *et al.*, Localize surface plasmon resonance of silver nanoparticles using Mie theory, *J. Mater. Sci.: Mater. Electron.*, 2023, **34**(32), 2128.
33 A. Chakravarty, *et al.*, Green synthesis of silver nanoparticles using fruits extracts of Syzygium cumini and their bioactivity, *Chem. Phys. Lett.*, 2022, **795**, 139493.
34 P. Pratim Sarma, K. Barman and P. K. Baruah, Green synthesis of silver nanoparticles using Murraya koenigii leaf extract with efficient catalytic, antimicrobial, and sensing properties towards heavy metal ions, *Inorg. Chem. Commun.*, 2023, **152**, 110676.
35 K. O. Saygi, H. M. Bayram and E. Bayram, Green synthesis of silver nanoparticles using artichoke flower petals and application in endodontic dentistry, *Biomass Convers. Biorefin.*, 2024, **14**(4), 5531–5539.
36 M. R. Matos, *et al.*, Green synthesis of silver nanoparticles and their application for colorimetric detection of L-cysteine: a spectroscopic investigation, *Inorg. Chem. Commun.*, 2024, **167**, 112767.
37 Y. Yadong and A. P. Alivisatos, Colloidal nanocrystal synthesis and the organic–inorganic interface, *Nature*, 2005, **437**(7059), 664–670.
38 V. Sharma, *et al.*, Influence of particle size and dielectric environment on the dispersion behaviour and surface plasmon in nickel nanoparticles, *Phys. Chem. Chem. Phys.*, 2017, **19**(21), 14096–14106.
39 M. A. Mahmoud, Effect of the dielectric constant of the surrounding medium and the substrate on the surface plasmon resonance spectrum and sensitivity factors of highly symmetric systems: silver nanocubes, *J. Am. Chem. Soc.*, 2012, **134**(14), 6434–6442.
40 V. Sharma, D. Verma and G. S. Okram, Influence of surfactant, particle size and dispersion medium on surface plasmon resonance of silver nanoparticles, *J. Phys.:Condens. Matter*, 2020, **32**(14), 145302.
41 O. A. Yeshchenko, Size-dependent surface-plasmon-enhanced photoluminescence from silver nanoparticles embedded in silica, *Phys. Rev. B*, 2009, **79**(23), 235438.
42 C.-T. Yang, Surface Plasmon Enhanced Light Scattering Biosensing: Size Dependence on the Gold Nanoparticle Tag, *Sensors*, 2019, **19**(2), 323.
43 B. Mekuye, The impact of size on the optical properties of silver nanoparticles based on dielectric function, in *Nanotechnology and Nanomaterials Annual Volume 2024*, IntechOpen, 2023.
44 K. Abe, Functional Group-Directed Photochemical Reactions of Aromatic Alcohols, Amines, and Thiols Triggered by Excited-State Hydrogen Detachment: Additive-free Oligomerization, Disulfidation, and C (sp2)–H Carboxylation with CO2, *J. Org. Chem.*, 2020, **86**(1), 959–969.
45 T. S. Maliehe, Chemical Profile, Antioxidant and Antibacterial Activities, Mechanisms of Action of the Leaf Extract of Aloe arborescens Mill, *Plants*, 2023, **12**(4), 869.
46 R. Padmavathi, *et al.*, Antioxidant and antimicrobial studies of silver nanoparticles synthesized via chemical reduction technique, *Mater. Today: Proc.*, 2022, **69**, 1339–1345.
47 L. D. S. M. Pinheiro, Silver nanoparticles from ascorbic acid: Biosynthesis, characterization, in vitro safety profile, antimicrobial activity and phytotoxicity, *Mater. Chem. Phys.*, 2024, **325**, 129715.
48 H. Wei, J.-L. Yang and Y.-P. Shi, Tannic acid-modified silver nanoparticles for antibacterial and anticancer applications, *ACS Appl. Nano Mater.*, 2023, **6**(11), 9617–9627.
49 V. Forest, M. Cottier and J. Pourchez, Electrostatic interactions favor the binding of positive nanoparticles on cells: A reductive theory, *Nano Today*, 2015, **10**(6), 677–680.
50 A. B. Lansdown, Silver in health care: antimicrobial effects and safety in use, *Curr. Probl. Dermatol.*, 2006, **33**, 17–34.
51 A. Chhatrapati Bisen, *et al.*, Chemical metabolite synthesis and profiling: Mimicking in vivo biotransformation reactions, *Bioorg. Chem.*, 2023, **139**, 106722.